RESEARCH ARTICLE

Structural Variants at the *LMNB1* Locus: Deciphering Pathomechanisms in Autosomal Dominant Adult-Onset Demyelinating Leukodystrophy

Paola Dimartino, PhD,[1†] Mariia Zadorozhna, PhD,[2†] Verónica Yumiceba, MSc,[3]
Anna Basile, MSc,[1] Ilaria Cani, MD,[4,5] Uirá Souto Melo, PhD [6,7] Jana Henck, MSc,[6]
Marjolein Breur, BSc,[8] Caterina Tonon, MD PhD,[4,5] Raffaele Lodi, MD,[4,5]
Alfredo Brusco, PhD [9,10] Tommaso Pippucci, PhD,[11] Foteini-Dionysia Koufi, MSc,[12]
Elisa Boschetti, PhD [12] Giulia Ramazzotti, PhD,[12] Lucia Manzoli, MD,[12]
Stefano Ratti, MD, PhD,[12] Filippo Pinto E Vairo, MD, PhD,[13]
Martin B. Delatycki, MD, PhD,[14] Giovanna Vaula, MD,[15] Pietro Cortelli, MD, PhD [4,5]
Marianna Bugiani, MD, PhD,[8,16] Malte Spielmann, MD [3,6,17] and Elisa Giorgio, PhD [1,2]

Objectives: We aimed to elucidate the pathogenic mechanisms underlying autosomal dominant adult-onset demyelinating leukodystrophy (ADLD), and to understand the genotype/phenotype correlation of structural variants (SVs) in the *LMNB1* locus.
Background: Since the discovery of 3D genome architectures and topologically associating domains (TADs), new pathomechanisms have been postulated for SVs, regardless of gene dosage changes. ADLD is a rare genetic disease associated with duplications (classical ADLD) or noncoding deletions (atypical ADLD) in the *LMNB1* locus.
Methods: High-throughput chromosome conformation capture, RNA sequencing, histopathological analyses of postmortem brain tissues, and clinical and neuroradiological investigations were performed.
Results: We collected data from >20 families worldwide carrying SVs in the *LMNB1* locus and reported strong clinical variability, even among patients carrying duplications of the entire *LMNB1* gene, ranging from classical and atypical ADLD to asymptomatic carriers. We showed that patients with classic ADLD always carried intra-TAD duplications,

resulting in a simple gene dose gain. Atypical ADLD was caused by *LMNB1* forebrain-specific misexpression due to inter-TAD deletions or duplications. The inter-TAD duplication, which extends centromerically and crosses the 2 TAD boundaries, did not cause ADLD. Our results provide evidence that astrocytes are key players in ADLD pathology.

Interpretation: Our study sheds light on the 3D genome and TAD structural changes associated with SVs in the *LMNB1* locus, and shows that a duplication encompassing *LMNB1* is not sufficient per se to diagnose ADLD, thereby strongly affecting genetic counseling. Our study supports breaking TADs as an emerging pathogenic mechanism that should be considered when studying brain diseases.

Autosomal dominant adult-onset demyelinating leuko-dystrophy (ADLD; OMIM# 169500) is a slowly progressing and fatal neurological disorder characterized by the symmetric demyelination of the central nervous system. Initial clinical symptoms generally occur in the fourth to fifth decades of life, with autonomic dysfunction preceding cerebellar and pyramidal signs.[1,2] ADLD is primarily associated with duplications encompassing the *LMNB1* gene (classical ADLD).[3,4] However, a second path to ADLD, involving deletions located upstream of the gene, with no involvement of the *LMNB1* coding sequence, has been described.[5,6] Interestingly, all patients with upstream deletions show clinical and neuroradiological differences from those with *LMNB1* duplications (atypical ADLD).[5,6]

Pathogenic mechanisms underlying ADLD are not entirely understood, but they directly involve lamin B1 accumulation in brain cells, leading to central nervous system demyelination.[7–9] Among the many unanswered questions regarding ADLD pathogenesis, the involvement of oligodendrocytes, astrocytes, or neurons in the disease mechanisms remains unclear. Moreover, the correlation between the genotype (gene duplication vs upstream deletion) and the phenotype observed in the patients is unknown. For duplications, a classic gene dosage mechanism has been postulated, which leads to overall *LMNB1* overexpression owing to the extra copy of the gene.[4] Accordingly, patients with duplications equally express 3 *LMNB1* alleles, suggesting the preservation of the regulatory context within the rearranged region.[4] Conversely, for patients carrying upstream deletions, an alteration of the *LMNB1* regulatory context has been hypothesized.[5,6] Data from a single family support the notion that deletions result in the removal of a crucial *LMNB1* regulatory element (enh-A),[5] and allow for interactions between the *LMNB1* promoter and foreign regulatory elements (enh-B; hs1371, hs1643, and hs1375) with a specific forebrain/midbrain expression pattern.[5,6] Preliminary results suggest that the atypical phenotype can be related to the enhancer-mediated misexpression of *LMNB1* in specific regions of the brain, such as the cerebrum (which is derived from the forebrain), but not in hindbrain-derived regions, including the cerebellum.[5] This phenomenon

needs to be further investigated and validated; however, it resembles a well-documented mechanism known as enhancer adoption or enhancer hijacking, which is predominantly associated with structural variants (SVs) that disrupt the integrity of topologically associating domains (TADs) and span TAD boudaries.[10–16] TADs act as regulatory units within the genome, mediating proper gene expression by restricting interactions between regulatory sequences, such as enhancers, and target genes within the TAD (Fig 1).[17]

In recent years, we have gathered information from >20 families with ADLD worldwide who carry *LMNB1* duplications, as well as from four families with *LMNB1* upstream deletions.

Here, we have described a significant variation in clinical symptoms among patients with *LMNB1* duplications. This range includes patients with classical ADLD, atypical ADLD, and completely asymptomatic individuals. Interestingly, all these patients carried 3 alleles of *LMNB1*, suggesting that an increase in gene copies alone cannot explain the observed phenotypic differences. This finding challenges the previously proposed theory of gene dosage as the sole mechanism underlying classical ADLD occurrence, thereby providing novel scenarios that need to be deciphered to offer proper clinical assessment to patients and their families.

SVs, including deletions or duplications, can have pathogenic effects owing to gene dosage changes and TAD structure disruption at a specific locus, resulting in gene misexpression (Fig 1). The development of chromosome conformation capture techniques has revolutionized this field, providing valuable tools to shed light on how TAD alterations can rewire enhancer–promoter interactions, ultimately leading to disease development.[10–16]

Here, we used genome-wide high-throughput chromosome conformation capture (Hi-C) techniques to samples from 7 individuals with SVs in the *LMNB1* locus to decipher the role of TAD alterations as a molecular mechanism underlying ADLD occurrence.

The present study supported enhancer adoption as a pathomechanism of upstream deletions, resulting in atypical ADLD. Moreover, we gained insights into the correlation between the genotype and phenotype in
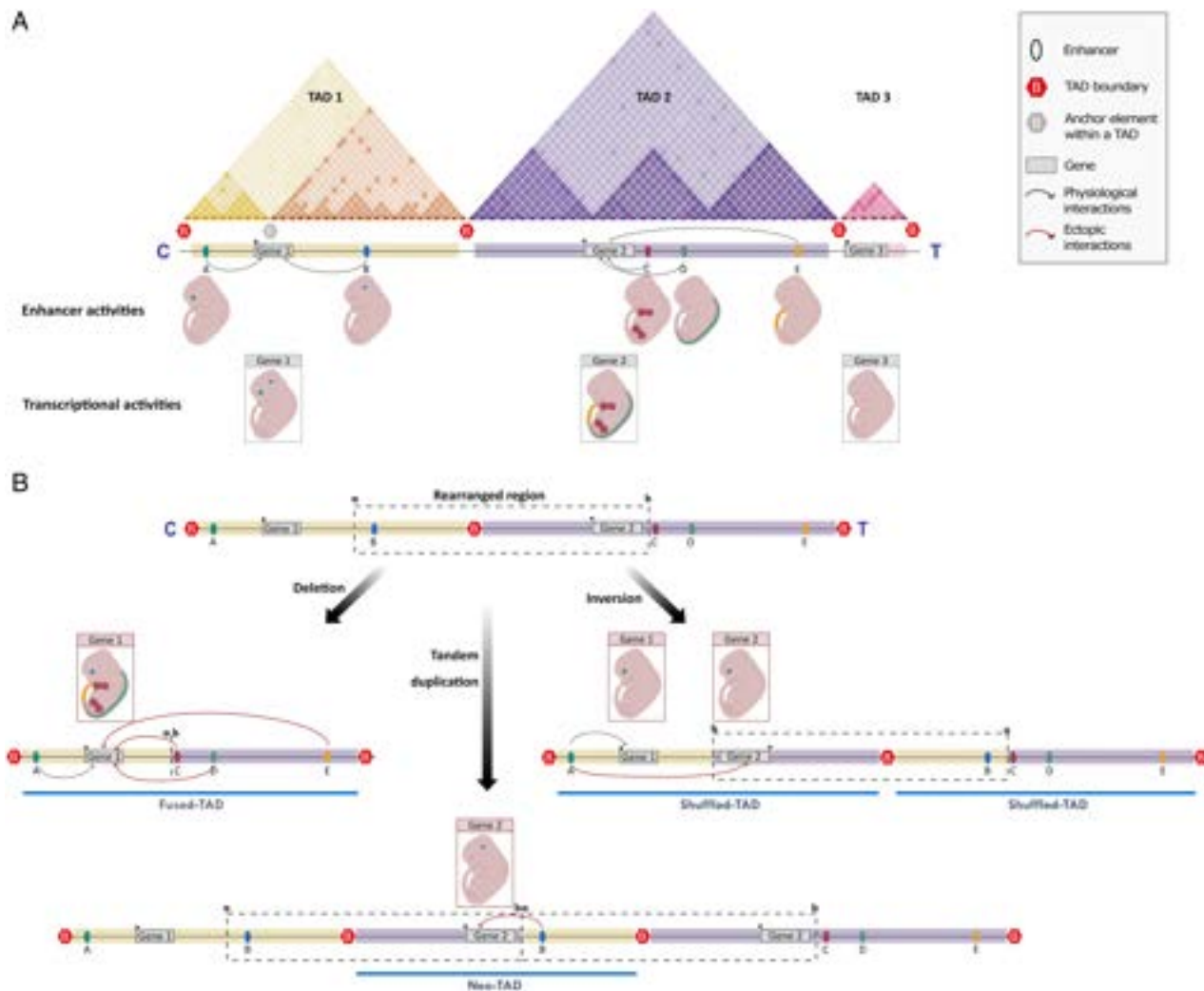
FIGURE 1: Topologically associating domains (TADs) and regulation of gene expression. TADs are stable and defined genomic regions delimited by insulating boundaries that act as regulatory units, confining time- and tissue-specific transcriptional activities. Regulatory interactions between long distance enhancers and gene promoters are favored by physically bringing these elements in close proximity. (A) An illustrative genomic locus with 3 genes (gray boxes) and 5 enhancers (colored ovals; A–E) organized into 3 TADs (TAD1 orange-, TAD2 purple-, and TAD3 pink-shaded triangles) is shown. TADs are physically separated by boundaries ("B" within red hexagons) formed by CTCF and cohesin complexes. Intra-TAD regulatory loops are mediated by anchor elements ("B" within gray hexagons) generating domains nested within larger TADs that are prone to change in a time- and tissue-specific manner. Enhancer-promoter interactions (arrows) are predominantly confined within a TAD. A hypothetical representation of how enhancer activity affects gene expression is reported. The regulatory activities of enhancers A–E in embryonic day 12.5 mouse embryos are represented in the diagrams above (enhancer activities). The resulting expression pattern of each gene driven by enhancers is illustrated in the diagrams below (gray boxes; transcriptional activities). In this example, enhancers A and B contribute to gene 1 transcription, whereas enhancers C–E contribute to gene 2 transcription. Gene 3 is repressed in all tissues at this embryological stage. (B) Structural variations (SVs) spanning TAD boundaries, genes and/or regulatory elements can, in addition to causing dosage effects, affect TAD structure and cause Mendelian phenotypes through aberrant expression patterns. The genomic region affected by the SVs (a-b, rearranged region) is highlighted (dotted line box) and encompasses the enhancer B, a TAD boundary, and the gene 2. These alterations can decouple a promoter from its cognate enhancers, resulting in a regulatory loss of function, while at the same time the adoption of new enhancers (red arrows) with different spatiotemporal activities might lead to ectopic gene activation (red boxes). Deletion: it causes a fused-TAD encompassing 2 adjacent domains, causing ectopic regulatory interactions and gene 1 mis-expression. Tandem duplication: it results in the creation of a new chromatin domain or neo-TAD. Here, the extra copy of the gene 2 loses its physiological enhancers (C–E) and it starts to interact with enhancer B, causing an aberrant expression pattern. Inversion: 2 shuffled-TADs are generated, and misexpression of gene 1 and gene 2 takes place due to the decoupling of gene promoters from their cognate enhancers (enhancer B for gene 1 and enhancers C, D, E for gene 2) and the simultaneous adoption of enhancer A by gene 2 promoter, resulting in an overlapping pattern of mis-expression of gene 1 and gene 2.

patients carrying *LMNB1* duplications. Our data suggested that widespread clinical variability is associated with different effects of duplications on the TAD structure

at the locus. Consequently, *LMNB1* duplication per se is not causative of ADLD, which potentially revolutionizes ADLD diagnosis and counseling. Finally, we addressed a

further fundamental unanswered question of what brain cell type is mainly involved in disease mechanisms, and provided evidence suggesting that astrocytes are key in ADLD pathology.

Materials and Methods

Samples

A group of 24 unique individuals carrying SVs at the *LMNB1* locus were included in this work, 21 of which have been already published (n = 17 duplications in Giorgio *et al.*[4] and Brunetti *et al.*[18]; n = 4 deletions in Giorgio *et al.*[5,6]). Biological samples were available for 10 ADLD cases from 8 unrelated families (Table). A total of 7 individuals carried a *LMNB1* duplication, whereas 3 had a deletion located upstream of the gene. Brain postmortem tissues were available for 2 patients (555–10, ADLD-1-TO VI-7), and primary dermal fibroblasts for 7 patients (IT3.3, IT3.4, IT4, A3, ADLD-1-TO VI-1, DEL1-1, BR1). DNA and RNA samples were available from a healthy individual carrying a large duplication spanning the *LMNB1* gene. All analyses were performed after obtaining informed consent. The study adhered to the Declaration of Helsinki standards, and was approved by the Ethics Committee of the IRCCS Mondino Foundation and Alma Mater Studiorum—Università di Bologna [Comitato Etico di Area Vasta Emilia Centro N° 160-2023-OSS-AUSLBO; EM-Em1-OSS-AUSLBO-23003-Em.1–367–2023-23,003].

Clinical and Neuroradiological Examinations

Italian ADLD patients (6 with a *LMNB1* duplication and 3 with a deletion located upstream of the gene; Table) were longitudinally evaluated at the Autonomic Unit of the IRCCS Istituto delle Scienze Neurologiche in Bologna (Italian ADLD reference center) through an extensive clinical and instrumental examination including: (1) clinical history and neurological examinations focused on autonomic symptoms, and cerebellar and pyramidal signs; (2) cardiovascular reflex test[19] and plasma noradrenaline levels to assess early cardiovascular autonomic dysfunction; (3) nerve conduction studies; and (4) neuropsychological evaluation. Brain magnetic resonance imaging (MRI) studies were performed following Zanigni *et al.*,[20] which includes metabolic and microstructural investigations. In some cases, it was possible to obtain consecutive brain MR studies to follow up the neuroradiological progression.

Genomic and Transcriptomic Analyses

Whole genome sequencing (NEBNext® Ultra™ II DNA Library Prep Kit; New England BioLabs, Ipswich, MA, USA) was performed to characterize the duplication identified in the asymptomatic family (sequencing outsourced to Personal Genomics srl, Italy; Supplementary Material). RNA from fibroblasts and whole blood samples was extracted using the Direct-Zol RNA MiniPrep system (Zymo Research, Irvine, CA, USA) and the PAXgene™ Blood RNA System Kit (Qiagen, Venlo, the Netherlands), respectively. RNA sequencing (RNA-seq) was performed on ADLD patients with *LMNB1* duplications (n = 4) or

upstream deletions (n = 2), a healthy individual carrying a large duplication spanning the *LMNB1* gene and 10 healthy controls, using the poly(A) mRNA capture and the NGS Stranded RNA Library Prep Set (Novogene, Beijing, China). Libraries were sequenced on a Novaseq X Plus (PE-150 bp; Illumina, San Diego, CA, USA), with ∼60 million fragments per sample. RNA-seq PE reads were mapped to the human genome build hs37d5 using Dragen (Illumina), and gene expression was retrieved using Dragen RNA pipeline (version 3.9.5; Illumina). Salmon quantification files were exploited to evaluate differentially expressed genes, using DRAGEN Differential Expression (v4.2.4; Illumina) based on the DESeq2 algorithm. We considered differentially expressed genes those genes that show an adjusted p value <0.001 and an absolute log2 fold change >2. A log2 fold change threshold of 0.75 was exploited to identify subtle alterations in expression.

Preparation of Hi-C Libraries

Hi-C experiments were performed on fibroblasts from ADLD patients with *LMNB1* duplications (n = 5) or upstream deletions (n = 2) and a healthy individual used as control in the analysis. Fibroblasts were cultured and grown to confluence to obtain ∼1 million cells to be fixed in 2% formaldehyde. Fixed cells were then lysed and digested using *DpnII* enzyme (R0543S; New England BioLabs). After digestion, restricted fragments were marked incorporating biotin-14-dATP during overhang fill-in (19524-016; Thermo Fisher Scientific, Waltham, MA, USA), and proximal ends were ligated overnight using T4 DNA ligase (M0202; New England BioLabs). To remove proteins holding interacting loci in close proximity, we reversed formaldehyde cross-linking with proteinase K digestion in presence of sodium dodecyl-sulfate 10% followed by a 4 hours of incubation at 68°C in 0.5 mol/L NaCl. DNA was purified by sodium acetate and ethanol precipitation. To prepare NGS sequencing libraries, biotinylated DNA was sonicated using Covaris (S-Series 220; Woburn, MA, USA), pulled down using Dynabeads MyOne Streptavidin T1 beads (65,602; Thermo Fisher Scientific), and end-repaired and phosphorylated using T4 DNA polymerase and T4 PNK (M0203 and M0201L; New England BioLabs). Finally, sequencing adaptors and indexes were added to DNA fragments using NEBNext Multiplex Oligos for Illumina kit (E7335 and E7500; New England BioLabs) and NEBNext Ultra II Q5 Master Mix (M0544; New England BioLabs). Double size selection of polymerase chain reaction products was performed using Agencourt AMPure XP beads (A63881; Beckman Coulter, Brea, CA, USA). Libraries were sequenced (∼240 million reads per sample) in a 75 bp paired-end run on a HiSeq4000 (Illumina).

Hi-C Bioinformatic Analysis

Hi-C data were processed using HiC-Pro v.3.1.0 with default options to obtain the coordinates of all valid interactions, starting from the raw fastq files. Reads were mapped to the GRCh37 reference build. HiC-Pro output was converted to Juicer format using an HiC-Pro accessory script. We used Juicer Tools v.1.22.01 and Straw v.0.0.8 to normalize Hi-C matrices with the

TABLE. Clinical Features of Italian Autosomal Dominant Adult-Onset Demyelinating Leukodystrophy Patients

Cases	Genotype	Age at onset (yr)	First system involved	Disease duration (yr)	Pyramidal sign (onset age; yr)	Dysarthria (onset age; yr)	Cerebellar ataxia (onset age; yr)	Dementia (onset age; yr)	Neurogenic OH (onset age; yr)	Urinary disturbance (onset age; yr)
IT3.1	*LMNB1* duplication	48	ANS	12	Yes (50)	Yes (51)	Yes (51)	No	Yes (49)	Yes (48)
IT3.3	*LMNB1* duplication	42	ANS, cerebellum	16	Yes (44)	Yes (49)	Yes (42)	No	Yes (42)	Yes (42)
IT3.2	*LMNB1* duplication	50	ANS	3	Yes (52)	Yes (54)	Yes (51)	No	Yes (50)	Yes (50)
IT3.4	*LMNB1* duplication	45	ANS	10	Yes (48)	Yes (47)	Yes (46)	No	Yes (46)	Yes (45)
IT6	*LMNB1* duplication	50	Pyramidal tract, cerebellum	10	Yes (50)	Yes (54)	Yes (50)	Yes (54)	Yes (52)	Yes (53)
IT5	*LMNB1* duplication	47	ANS	12	Yes (51)	No	Yes (55)	No	Yes (57)	Yes (47)
delITA 131679	*LMNB1* deletion	47	Pyramidal tract	3	Yes (47)	Yes (47)	No	No	No	No
delITA 1351FF	*LMNB1* deletion	42	Pyramidal tract	4	Yes (42)	Yes (48)	No	No	No	No
delITA A922	*LMNB1* deletion	42	Cerebellar pathways	8	Yes (45)	Yes (48)	No	No	No	No

Onset ages are reported in years. Abbreviations: ANS: autonomic nervous system; OH: orthostatic hypotension.

Knight-Ruiz (KR) matrix balancing algorithm and extract chromosome 5 cis interactions at 10 kb resolution, respectively. Hi-C maps were visualized as heatmaps rotated by 45°, and compared with cell-type matched controls. Case versus control subtraction method was used to highlight gain or loss of cis contacts in patients Hi-C maps.

Histopathological Analysis of Brain Samples

Autopsy was performed in 2 ADLD patients: 555–10 (classical ADLD) and ADLD-1-TO VI-7 (atypical ADLD; from Giorgio et al.[5]) at the Amsterdam University Medical centers, the Netherlands, and at Maria Vittoria Hospital, Torino, Italy, respectively. Brain tissue samples from the frontal and cerebellar white matter of 2 age-matched controls without confounding neuropathology was also used. Formalin-fixed paraffin-embedded 5-μm thick tissue sections were routinely stained with hematoxylin–eosin. Slides were deparaffinized, rehydrated, and incubated in 0.3% (w/v) H_2O_2 in dH_2O for 30 min to block endogenous peroxidase activity. Heat-induced antigen retrieval was carried out in 10 mmol/L citrate buffer (pH 6.0) or 10 mmol/L Tris 1 mM ethylenediaminetetraacetic acid buffer (pH 9.0). Primary antibodies against the Lamin B1 (LMNB1, 1:100; Abcam, Cambridge, UK; ab16048), the astrocyte-specific marker glial fibrillary acidic protein (GFAP; 1:1000; Dako, Glostrup, Denmark; Z0334), and macrophage/monocytes marker (CD68, 1:500; Dako; M0814) were incubated overnight at room temperature. The next day, slides were rinsed and incubated with horseradish peroxidase labeled secondary antibodies. Immunopositivity was detected using 3,3′-diaminobenzidine chromogen. Light microscopy pictures were taken with a Leica DM6000B microscope (Leica microsystems, Wetzlar, Germany). Immunohistochemical stains for CD68 and LMNB1 were blindly evaluated by manually recording the number of positive cells (immunopositive cells per mm^2) from five serial ×200 sections of autopsy tissue for each specimen by 3 experienced pathologists.

Databases and In Silico Analysis

We evaluated the epigenetic landscape of the *LMNB1* locus in 10 different cell types using the UCSC browser (https://genome.ucsc.edu), selecting the ENCODE/Broad Institute CHIP-seq data tracks for CTCF, H3K27ac, H3K4me1, H3K4me3, and H3K9me3. TAD boundaries were established after evaluating the CTCF marker and already published Hi-C maps available at the 3D Genome Browser (3dgenome.fsm.northwestern.edu). We investigated the VISTA Enhancer Browser (https://enhancer.lbl.gov) for regions with enhancer activity. Briefly, we selected human noncoding regions within the *LMNB1* locus that were

classified as positive enhancers. A positive enhancer is a region showing reproducible tissue-specific reporter expression in at least three transgenic embryos (E11.5), each representing an independent oocyte injection throughout the transgenic mouse enhancer assay. Finally, we evaluated gene expression in different regions of the brain exploiting RNA consensus tissue gene data from the Human Protein Atlas database (https://www.proteinatlas.org/). For our genes of interest, we downloaded normalized Transcripts Per Million values, representing consensus transcript expression levels per gene in 50 tissues based on transcriptomics data from HPA and GTEx.

Results

Comparison of Clinical and Neuroradiological Features in ADLD Cases with LMNB1 Duplications versus Upstream Deletions

Clinical features of nine Italian patients with ADLD are summarized in Table. ADLD cases with *LMNB1* duplications are generally reported with a classical and clinically homogeneous form of disease (classical ADLD). However, it is known, and further confirmed in the present study, that individuals with *LMNB1* duplication are different from those with a deletion upstream of the gene, who do not show an early involvement of autonomic nervous system with neurogenic orthostatic hypotension and urinary dysfunction or cerebellar ataxia, but instead they have predominant pyramidal signs (atypical ADLD). MRI also confirmed a difference between patients with classical and atypical ADLD, showing a selective involvement of cerebral white matter with sparing of cerebellar and bulbar myelin at MRI in the latter (Fig 2).

Moreover, in the past 15 years, we collected 20 families worldwide carrying a *LMNB1* duplication, and we noticed a marked clinical variability. Indeed, we identified 17 patients with a canonical phenotype (classical ADLD), a case who phenotypically more closely match the picture of patients with deletions (atypical ADLD), and finally, an individual carrying a large duplication spanning the *LMNB1* gene, who had neither clinical nor neuroradiological signs despite being far above the age of onset (68 years; asymptomatic carrier; Suppl material). This observation requires a novel explanation of the pathogenic mechanism mediated by duplications at the *LMNB1* locus.

Classification of Duplications and Deletions at the LMNB1 Locus

Deletions encompassing a TAD-boundary caused a fused-TAD in which ectopic regulatory contacts can occur.[17,21] A recent article demonstrated that duplications can also alter the 3D genome architecture and the TAD structure, leading to different phenotypes depending on their nature (intra-TAD duplications or inter-TAD duplications).[11]

We hypothesized that the 3 clinical phenotypes associated with *LMNB1* duplications can be explained by a similar mechanism.

The physiological TAD structure at the *LMNB1* locus was achieved by exploiting Hi-C data from fibroblasts obtained from a healthy individual (Fig 3). The Hi-C map showed 3 different TADs at the locus. The first TAD was ≈950 Kb in size and included the *LMNB1* gene, its regulatory element (already characterized,[5] named "Enh A"), and 3 other OMIM genes, namely *PHAX*, *MARCHF3*, and *MEGF10*. The contiguous, centromeric 2.96 Mb TAD encompassed *ZNF608*, *GRAMD3*, and *ALDH7A1*, and contained an extended gene desert with 4 enhancer regions with a midbrain/forebrain activity (from VISTA Enhancer Browser and Giorgio *et al*.[5]). The neighboring TAD was 1.68 Mb in size, and included *SRFBP1*, *LOX*, *SNCAIP*, *SNX2*, *PPIC*, *PRDM6*, *CEP120*, and *CSNK1G3* OMIM genes.

Based on the size and the inclusion or not of TAD boundaries, duplications encompassing the *LMNB1* gene could be classified as: (1) intra-TAD duplications not affecting a boundary, (2) inter-TAD duplications encompassing a TAD boundary, and (3) inter-TAD duplications encompassing 2 consecutive boundaries. On the contrary, all deletions so far reported in ADLD patients are inter-TAD deletions eliminating a TAD boundary (Fig 3).

Interestingly, all 17 classical ADLD cases carried an intra-TAD duplication; namely, the duplication was totally contained within the *LMNB1* TAD and did not extend beyond its boundaries (Fig 3A), whereas atypical ADLD patients could have either an inter-TAD duplication (Fig 3B) or inter-TAD deletions (Fig 3C) encompassing the boundary between the *LMNB1* TAD and the adjacent one. Finally, the asymptomatic individual carried an inter-TAD duplication spanning *LMNB1* and the 2 centromeric TAD-boundaries (Fig 3D; Supplementary Material).

In Silico Evaluation of the LMNB1 Locus

In silico evaluation of the TAD structure at the *LMNB1* locus showed that it was highly conserved among human tissues. As expected, anchor points differed in a cell-specific manner (Fig S1A), thus potentially generating sub-TAD compartmentalization and tissue-specific regulatory contacts.

The in silico prediction of regulatory elements (DNase I Hypersensitive and H3K27ac positive regions) coupled with functional validation by performing a mouse transgenic enhancer assay (VISTA enhancer browser) allowed the identification of 4 enhancer regions in the *LMNB1* locus. All these enhancers were located within
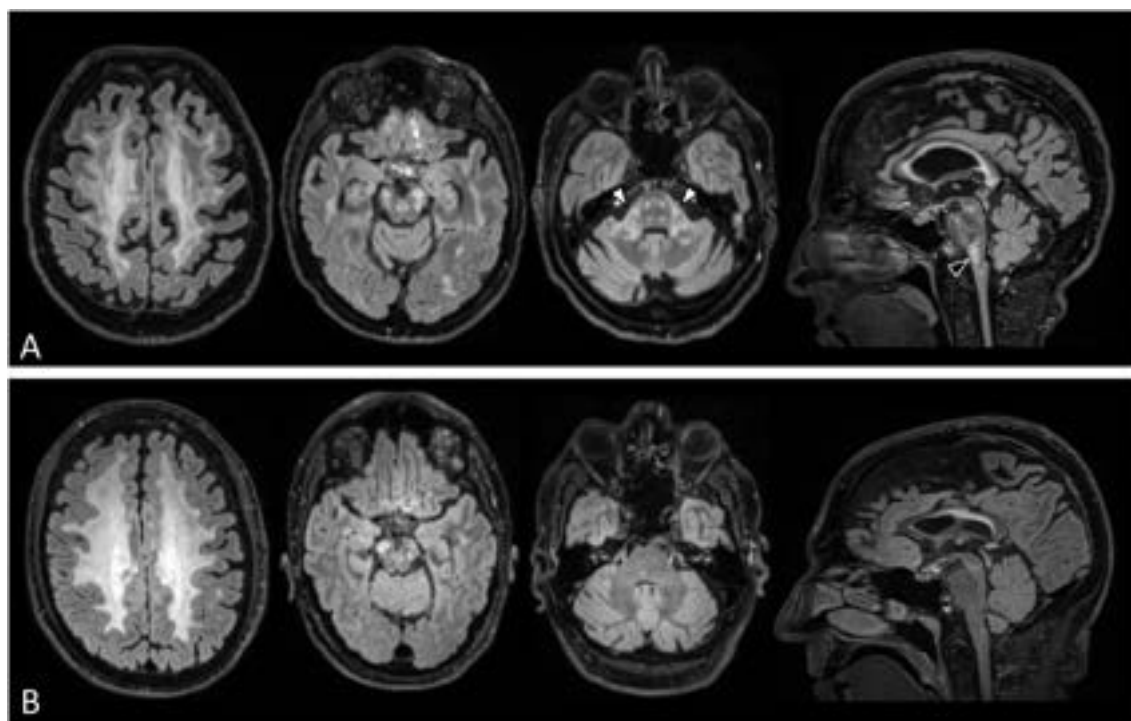
FIGURE 2: Brain magnetic resonance imaging features in patients with *LMNB1* duplications versus patients with deletions upstream of *LMNB1*. Axial and sagittal fluid attenuated inversion recovery images of a patient with a *LMNB1* duplication (IT6, panel A) and a patient with a deletion upstream of *LMNB1* (delITA A922, panel B). Both participants demonstrate widespread hyperintensity of supratentorial white matter and cerebral peduncles, but only the patient with the *LMNB1* duplication shows involvement of the middle cerebellar peduncles (white arrowheads) and of the bulbar pyramids (black arrowhead).

the *GRAMD3* TAD and showed a midbrain/forebrain pattern of expression (Fig S1B,C). Based on the assumption that genes within a TAD share regulatory elements and consequently show similar patterns of expression, we investigated the physiological RNA expression of target genes in different brain tissues (hindbrain- vs forebrain-derived; data from the Human Protein Atlas database). The physiological *LMNB1* expression pattern varied among the brain tissues, with a higher level in hindbrain-derived regions, such as the cerebellum, than in the forebrain- and midbrain-derived tissues and spinal cord. Conversely, *ALDH7A1* and *GRAMD3* were predominantly expressed in the forebrain/midbrain-derived regions and spinal cord compared with their expression in the cerebellum (Fig S1D), which was consistent with the pattern of the activity of 4 enhancers located within the same TAD (hs1375, hs1643, hs1371, and hs2325; Fig S1). Genes located in the most centromeric TAD showed very low expression in the brain, with the only exception of *SNX2* (Fig S1D).

Hi-C Dissects TAD Structure Alterations at the LMNB1 *Locus*

We performed Hi-C on fibroblasts from 7 ADLD patients and a healthy individual to further investigate the effects of SVs in the *LMNB1* locus on the 3D genome organization and TAD structure. The Hi-C map from a healthy individual was used as a control (Fig 4A). Following the classification previously proposed, we grouped patients depending on the nature of the SV carried.

Cases with intra-TAD duplications (Figs 3A and 4B; Supplementary Fig S2B–D; Table S2). Patients IT3.3 and IT3.4 were relatives, and shared a 325 kb *LMNB1* tandem duplication. This copy number gain started few kilobases upstream of the *LMNB1* gene and extended telomerically, affecting the 3′ UTR of *MARCH3*. Patients A3 and IT4 had smaller tandem duplications. Patient IT4 carried the smallest duplication so far reported that included the *LMNB1* gene only (Fig 3A). In all these cases, the Hi-C maps showed the copy number gains as an increase of interactions within the duplicated region. The subtraction method from control versus IT3.3 (Fig 4B), IT3.4 (Fig S2B), A3 (Fig S2C), or IT4 (Fig S2D) further revealed the tandem duplications as a strong gain of contact between the beginning and the end of the duplicated regions. In all the Hi-C maps, the duplications occurred within the physiological *LMNB1* TAD without affecting the overall 3D genome structure, and did not include the *LMNB1* physiological regulatory element.[5]

7
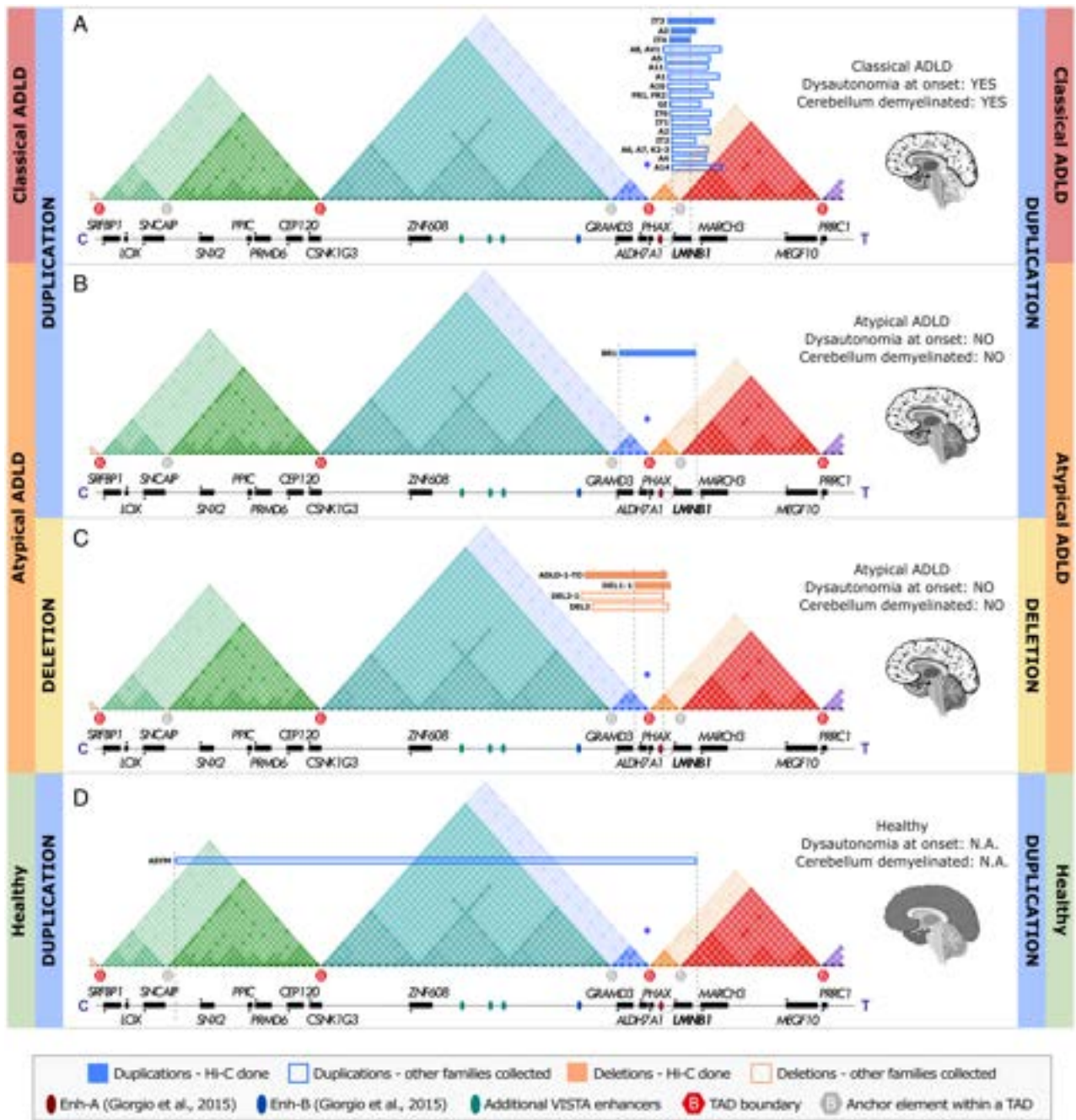
FIGURE 3: Structural variants (SVs) at the *LMNB1* locus and associated phenotypes. A schematic representation of the topologically associating domain (TAD) structure at the *LMNB1* locus is shown. The minimal duplicated/ deleted region is reported for each participant based on array comparative genomic hybridization results (light blue or orange rectangles, respectively). Solid rectangles: participants analyzed by high-throughput chromosome conformation capture (Hi-C); void rectangles: participants not analyzed by Hi-C. Our cohort of 24 SVs at the *LMNB1* locus has been subdivided in 4 groups based on the SV type (duplications vs deletions), the crossing or not of TAD boundary/ies, and the clinical and neuroradiological phenotypes (classical ADLD, atypical ADLD, healthy). For each group, the critical region is highlighted by dashed lines. (A) Classical ADLD cases carry an intra-TAD duplication (n = 17). Here, the extra *LMNB1* copy is in the native domain and therefore maintains its physiological regulatory context, resulting in gene overexpression. Patients with atypical ADLD carrying either (B) an inter-TAD duplication or (C) inter-TAD deletions (n = 4), causing the relocation of a *LMNB1* allele in an equivalent regulatory context and in turn causing *LMNB1* misexpressions in the brain of patients. (D) The asymptomatic individual carries a duplication encompassing 2 consecutive boundaries. Here, based on the TAD structure, we assume that the *LMNB1* extra copy is relocated in a foreign regulatory context within the green TAD, likely preventing its expression in at least the brain of the carriers. ADLD = Autosomal Dominant Adult-Onset Demyelinating Leukodystrophy; N.A. = not applicable.

Cases with inter-TAD duplications (Figs 3B and 4C; Table S2). Patient BR1 had a 475 kb inverted duplication already characterized at the nucleotide level by our group (Fig S3).[4] This rearrangement encompassed the *LMNB1* gene as for the intra-TAD group, but extended centromerically, including the boundary and part of the contiguous TAD (Fig 3B). In the Hi-C map, the rearranged region showed an overall increase of contacts, and it was characterized by a red stripe at the telomeric end of the duplicated region, indicating ectopic interaction between the *LMNB1* TAD and the neighboring domain. Moreover, Hi-C highlighted the formation of a neo-TAD encompassing the extra copy of the *LMNB1* gene, the physiological regulatory element[5] and its extra copy, and a shuffled-TAD, where ectopic interactions took place. The shuffled TAD included the non-duplicated *LMNB1* allele and, interestingly, due to the inversion, the *ALDH7A1* gene, a portion of the *GRAMD3* gene, and potentially their regulatory elements (Fig 4C).

Cases with inter-TAD deletions (Figs 3C and 4D; Figs S2E; S4A; Table S2). Patient ADLD-1-TO VI-1 carried a 660 kb deletion, extending 66 kb upstream of the *LMNB1* promoter toward the centromeric boundary. The deletion included 3 OMIM coding genes, namely *PHAX*, *ALDH7A1*, and *GRAMD3*, a TAD boundary, and the *LMNB1* physiological regulatory element.[5] Patient DEL1-1 had the smallest deletion so far reported, encompassing only the *LMNB1* physiological regulatory element, the TAD boundary, and *PHAX* and *ALDH7A1* genes (Fig 3C). The Hi-C maps showed loss of contacts between the beginning and the end of the rearrangements as a characteristic V-shape signal, and a gain of interactions starting from the deletion breakpoints toward the whole contiguous TAD. The subtraction method from control versus ADLD-1-TO VI-1 (Fig 4D) and DEL1-1 (Fig S2E) further highlighted the V-shaped loss of contacts and the ectopic interactions as an intense red stripe, clearly indicating an enhancer adoption mechanism, as previously described,[5,6] and demonstrating the formation of a fused-TAD. A similar mechanism could be postulated for all inter-TAD deletions, so far reported (Fig S4A).

Notably, Hi-C allowed for the detection of breakpoints of all rearrangements analyzed with a resolution comparable to that of high-density oligonucleotide arrays, which are currently the gold standard technique for CNV detection (Table S2). Moreover, Hi-C resolved the inverted duplication carried by patient BR1, which was seen as just a copy number gain by array-based techniques.

RNA-Seq

We performed RNA-seq expression analyses as a possible readout of TAD structure alterations identified by Hi-C.

All genes located within the *LMNB1* locus were non-differentially expressed in patients compared with their expression in controls, including genes directly involved in CNVs (eg, *LMNB1* in patients with classical ADLD),[8] with the only exception of *PHAX* and *MARCH3*, which were downregulated in ADLD-1-TO (Fig S5). Nevertheless, the transcript quantification results showed that in patients with classical and atypical ADLD, *LMNB1* was overexpressed compared with its expression in controls.[4,5] Moreover, in atypical ADLD cases carrying a deletion upstream of the gene, *GRAMD3*, *ALDH7A1*, and *PHAX* downregulation was reported (Figs S5 and S6). Finally, the BR1 sample did not show *PHAX* and *ALDH7A1* overexpression, even though they were fully encompassed by the inverted duplication. However, misexpression needs to be observed in disease-relevant tissues based on enhancers tissue-specificity, namely the brain of the patients.

Histopathological Evaluation of ADLD Brain Samples Unravels Phenotypic Differences in Patients with LMNB1 Duplications versus Upstream Deletions

To corroborate enhancer-mediated misexpression in specific brain regions, and to further evaluate the correlation between *LMNB1* overexpression/misexpression and the neuropathology,[5] we performed an examination of postmortem brain samples from a patient with classical ADLD carrying a tandem intra-TAD duplication (555–10) and a patient with atypical ADLD carrying an *LMNB1* upstream deletion (ADLD-1-TO VI-7 from Giorgio et al.[5]; Fig 5; Table S1).

The neuropathology in the cerebral white matter of both patients was very similar, showing the involvement of the deep white matter with the relative sparing of U-fibers and the deepest periventricular areas. A patchy lack of myelin with myelin preservation around blood vessels was observed and was associated with a normal density of oligodendrocytes. There was little, if any, inflammation, with scarce microglia, no infiltrating lymphocytes, and only some CD68/CD163-positive macrophages around blood vessels where the myelin was better preserved (Figs 5S–X and S7A).

Notably, the lack of lipid-laden macrophages contradicted demyelination and suggested diffuse white matter degeneration. Virtually no reactive gliosis was observed in the presence of scarce dysmorphic astrocytes with short and blunt cell processes.

LMNB1 staining revealed the preservation of nuclear membranaceous immunoreactivity in the patient with classical ADLD. Interestingly, we noticed presumably stronger *LMNB1* immunoreactivity in the cerebellar white
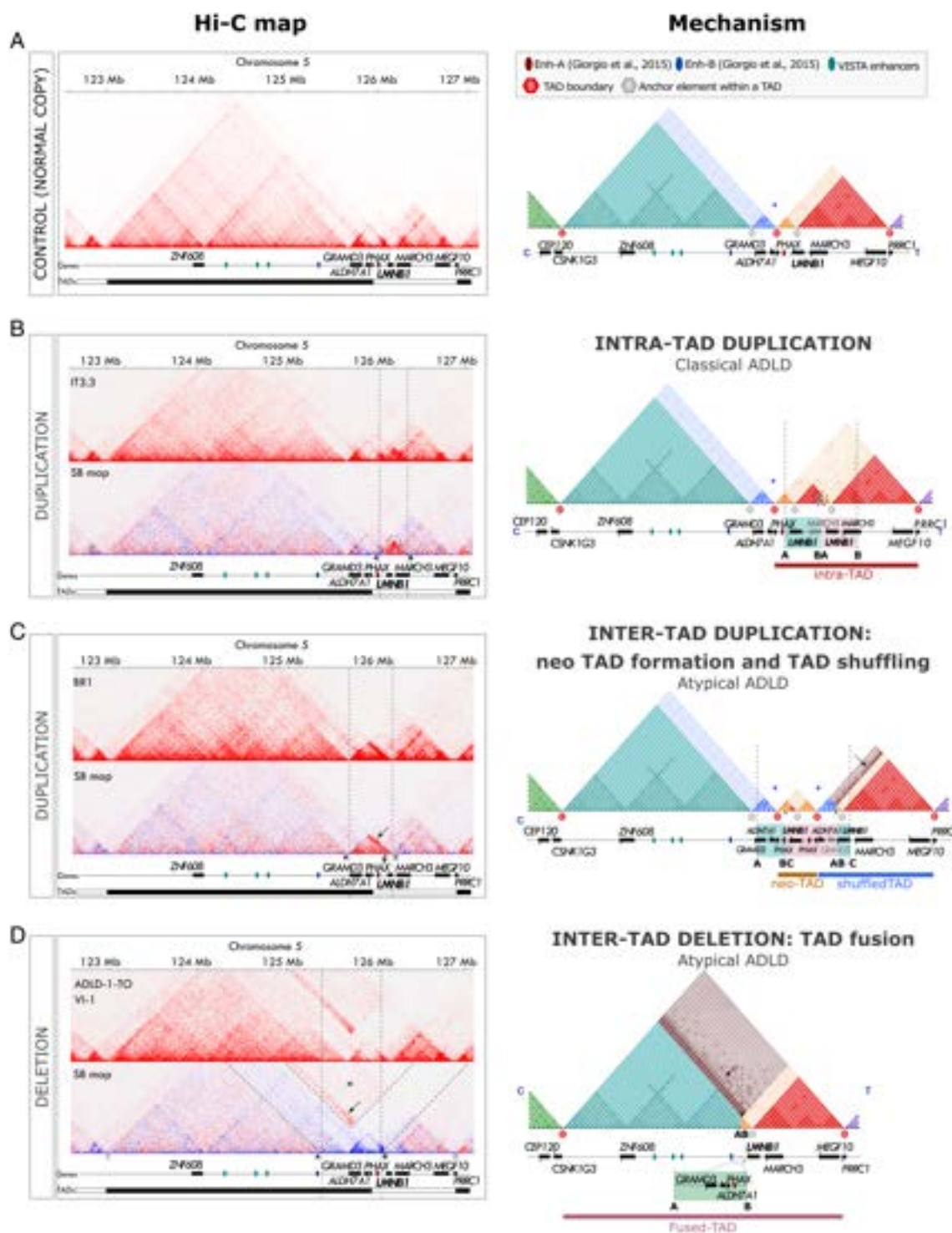
FIGURE 4: High-throughput chromosome conformation capture (Hi-C) maps unveils pathomechanisms of structural variants (SVs) at the *LMNB1* locus. Hi-C heatmaps of the *LMNB1* locus and their graphical representations (right panels) are shown (skin fibroblast; hg19; 10 kb resolution; raw count map). For patients, a second heatmap obtained with the subtraction method (SB map; patient-control) is reported. (A) Hi-C heatmap from a healthy individual shows the physiological TAD structure at the *LMNB1* locus (*LMNB1* TAD in red; *ALDH7A1*, *GRAMD3*, and *ZNF608* TAD in light blue; *CEP120* TAD in green). (B) Hi-C and SB map from IT3.3 patient with a 325 kb *LMNB1* tandem duplication highlighted with dot lines. The SB map emphasized the duplicated region as gain of interactions (red triangle; in SB map, A and B pointed out the 2 breakpoints; dot circle shows the point of maximum interaction between A and B, corresponding to the new BA junction). On the right: the cartoon shows the linear representation of the allele carrying the duplication (the native and the extra *LMNB1* copies are highlighted in light blue and pink in the gene track below the respective map, respectively). The dot circle shows the point of maximum interaction between A and B. The SV causes an intra-TAD duplication. Of note, *LMNB1* physiological regulatory element is not included in *(Figure legend continues on next page.)*

matter of the patient with the duplication than in the control and atypical case (Figs 5J–L and S7B). Accordingly, notable differences were observed in cerebellar white matter pathology between the 2 examined patients. In the patient with classical ADLD, the cerebellar white matter was severely affected, with tissue rarefaction, lack of myelin, and meager reactive gliosis with dysmorphic astrocytes. Conversely, in the patient with atypical ADLD, the cerebellar white matter was relatively spared, with no tissue rarefaction, normal myelin staining, and morphologically normal astrocytes. Interestingly, *LMNB1* expression was negligible (Figs 5L and S7B). Based on these findings, we speculated that astrocytic pathology covaries with the severity of white matter neuropathology and possibly with lamin B1 levels (Fig 5).

Discussion

Human development results from the complex process of gene expression in some cell types and not in others at specific times during development through various gene regulatory elements, including enhancers. Enhancers physically contact target promoters to effect time- and tissue-specific transcriptional activation. Multiple enhancer–promoter interactions occur within TADs. DNA folding and regulatory activity within a single TAD are separated from neighboring TADs by boundaries or insulators. Overall, TADs are the regulatory backbone of the genome and functional units (Fig 1). Additionally, different Mendelian phenotypes are associated with alterations in the regulatory control of genes and/or disruption of TAD structures.[22]

Deletions, duplications, and inversions can alter the *cis*-regulatory 3D architecture of the genome by changing the position of boundaries and gene regulatory elements of TADs, thus leading to pathological phenotypes that are not directly correlated to gene dosage alterations.[11,17,21,23] Most reported examples are skeletal malformations and certain tumors,[11,21–24] but very few brain diseases have been described.

ADLD[4] (OMIM#169500) is a neurological disease associated with coding and noncoding SVs in the *LMNB1* locus. Duplications encompassing *LMNB1* are associated with the classical ADLD phenotype,[4] whereas deletions located upstream of *LMNB1* are present in atypical ADLD cases with clinical and neuroradiological peculiarities. These findings are consistent with an alteration in the *LMNB1* regulatory context, resembling an enhancer adoption mechanism,[5,6] which should be further investigated and validated. No detailed phenotypic characterization has been reported; thus, we performed an extensive clinical and neuroradiological investigation of 6 patients with classical and 3 patients with atypical ADLD to understand the neuropathological course in both groups.

Compared with classical ADLD patients, atypical ADLD patients present with neither early involvement of the autonomic nervous system nor cerebellar ataxia. MRI showed the selective involvement of the cerebral white matter, whereas the cerebellar and bulbar myelin was spared. The results corroborate the clinical variability described in ADLD patients carrying a deletion upstream of *LMNB1* compared with those carrying a gene duplication.[5,6]

We are the first to report strong phenotypic variability, even among patients carrying *LMNB1* duplications, ranging from classical and atypical ADLD to asymptomatic carriers. All patients carried 3 *LMNB1* copies; therefore, an increase in gene dosage could not explain the emerging clinical complexity. The classification of all deletions and duplications identified in our cohort based on their sizes and effects on the 3D genome architecture, coupled with Hi-C, helped elucidate pathogenic mechanisms underlying ADLD and understand the genotype/phenotype correlation of SVs in the *LMNB1* locus.

Patients with classical ADLD carried intra-TAD duplications that did not affect a boundary, where the *LMNB1* extra copy was in the native domain and maintained its physiological regulatory context, resulting

---

the duplication (C) Hi-C and SB map from BR1 patient with a 475 kb inverted duplication highlighted with dot lines (A and C pointed out the 2 breakpoints; B corresponds to the breakpoint where the duplicated region is inserted). The red stripe indicates the formation of new ectopic interactions (arrow). On the right: the illustration shows the linear representation of the allele carrying the duplication. The rearrangement causes the formation of a neo-TAD with the extra copy of the *LMNB1* gene (in pink in the gene track below), and 2 copies of *LMNB1* physiological element, and a shuffled-TAD with the native LMNB1 copy (in light blue in the gene track below) and regulatory elements from the adjacent TAD. Interestingly, due to the inversion, the shuffled TAD also includes 2 coding genes from the adjacent TAD, namely the *ALDH7A1* gene and a portion of the *GRAMD3* gene. The arrow points out the new ectopic interactions. (D) Hi-C and SB map from ADLD-1-TO VI-1 patient carrying a 660 kb deletion located upstream of the *LMNB1* gene highlighted with dot lines. The SB map emphasized the deleted region as a V-shaped signature (dashed lines; A and B pointed out the 2 breakpoints). An overall increase in interactions between C and D is clearly stated (asterisk), suggesting a fused-TAD. The red stripe indicates the formation of new ectopic interactions between the *LMNB1* promoter and regulatory elements physiologically located in the adjacent TAD (arrow, enhancer adoption). On the right: the illustration shows the linear representation of the allele carrying the deletion (in light green in the gene track below). The rearrangement causes the loss of a TAD boundary and the fusion of the 2 adjacent TADs (fused-TAD).
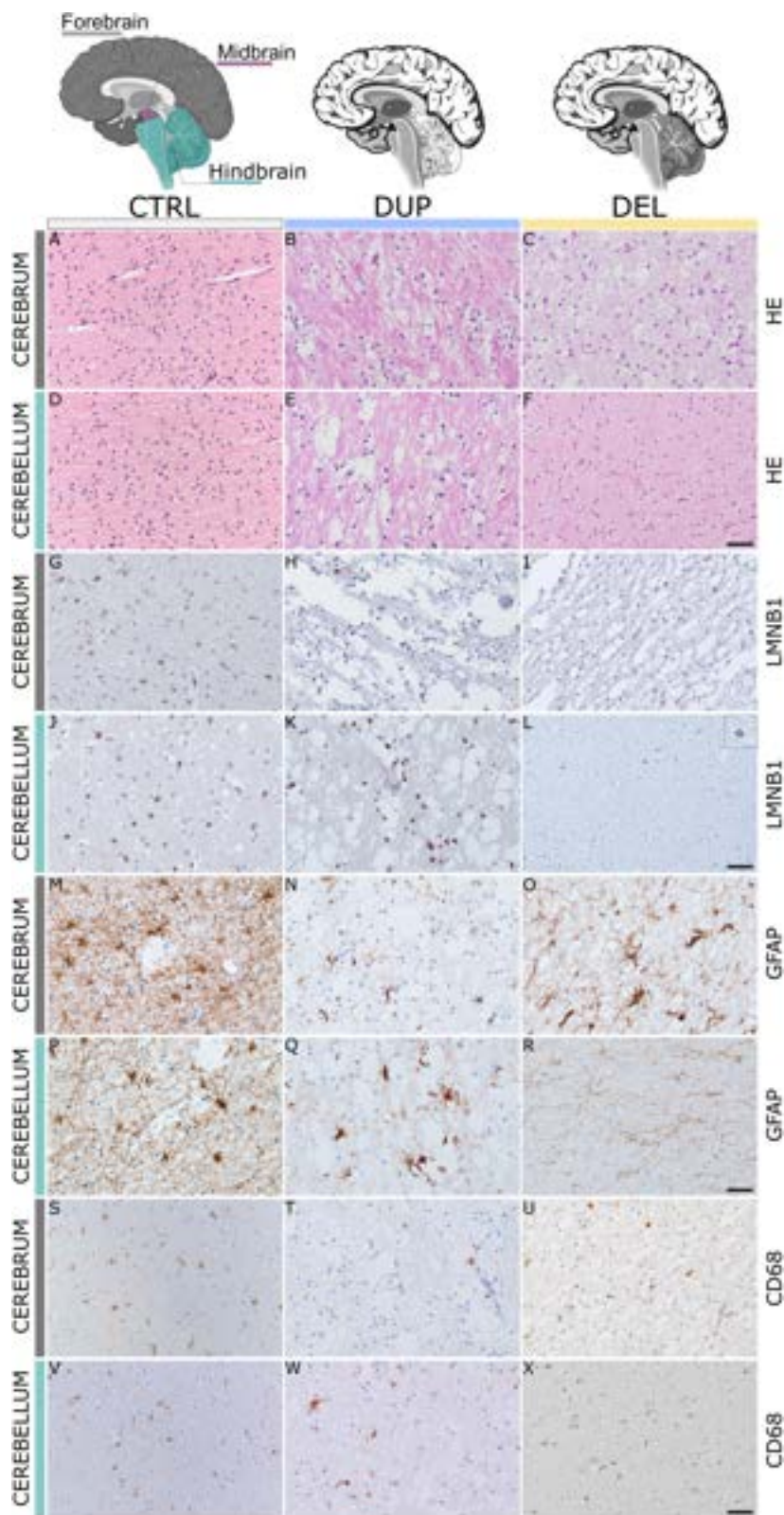
FIGURE 5: Pathology of Autosomal Dominat adult-onset demyelinating LeukoDystrophy (ADLD). Postmortem obtained frontal white matter from the second frontal gyrus (CEREBRUM, grey rectangles) and postmortem obtained cerebellar white matter located between the nucleus dentatus and the inferior cortex (CEREBELLUM, light blue rectangles) from a healthy control (CTRL), the 555–10 patient carrying an intra-TAD duplication (DUP) and the ADLD-1-TO VI-7 patient (Giorgio *et al.*, 2015) carrying a deletion upstream of the *LMNB1* gene (DEL) are shown. A schematic representation of forebrain-, hindbrain-, and midbrain-derived regions of brain, and of neuroradiological findings of classical and atypical ADLD patients is shown. Slides have *(Figure legend continues on next page.)*

in gene overexpression. Interestingly, none of the duplications associated with classical ADLD included the *LMNB1* physiological regulatory element.[5] *LMNB1* misexpression caused atypical ADLD owing to inter-TAD deletions or the inter-TAD duplication. In the first group, Hi-C supported enhancer adoption as the disease occurrence mechanism.[5,6] All deletions reported encompassed the cognate TAD boundary, resulting in a fused TAD where the *LMNB1* allele freely interacted with forebrain/midbrain enhancers physiologically located in the neighboring domain. Notably, ectopic chromatin contact formation between the same adjacent domain and the *LMNB1* allele has been demonstrated for the inter-TAD inverted duplication. The Hi-C map showed ectopic interactions due to shuffled TAD formation (Fig 4C). Owing to the inversion, *ALDH7A1* and a portion of *GRAMD3* were relocated in the shuffled TAD together with a *LMNB1* allele, potentially allowing *ALDH7A1/GRAMD3* regulatory elements to hijack the *LMNB1* promoter.

We used RNA-seq expression data as a possible proxy for the TAD structure alterations identified by Hi-C (Fig S5). No differentially expressed genes were detected in the *LMNB1* locus, except for *PHAX* and *MARCH3* that were downregulated in ADLD-1-TO. The transcript quantification results showed *LMNB1* overexpression in all ADLD patients,[4,5] and *GRAMD3*, *ALDH7A1*, and *PHAX* downregulation in ADLD-1-TO and DEL1-1 cells. The 3 genes were deleted in ADLD-1-TO, whereas DEL1-1 deletion encompassed *ALDH7A1* and *PHAX* (Figs S5 and S6). Finally, neither *PHAX* nor *ALDH7A1* were overexpressed in the BR1 sample, even if they were fully duplicated by the inverted duplication. In atypical ADLD patients, *PHAX*, *ALDH7A1*, and/or *GRAMD3* were probably misregulated due to the TAD structure alteration (inter-TAD deletion or duplication) and the resulting change in their regulatory contexts (Figs S5 and S6). *LMNB1* was physiologically more highly expressed in hindbrain-derived tissues than in forebrain/midbrain-derived tissues and the spinal cord, whereas

GRAMD3 and *ALDH7A1* showed the opposite pattern of expression, as they were more highly expressed in forebrain-/midbrain-derived tissues (Fig S1D), consistent with the pattern of activity of the 4 enhancers located within the same TAD (Fig S1B,C). The clinical and neuroradiological similarities between patients carrying inter-TAD deletions or duplication were attributed to the relocation of an *LMNB1* allele in an equivalent regulatory context (*GRAMD3*- and *ALDH7A1*- specific) and the simultaneous loss of its physiological regulatory element, causing overlapping *LMNB1* misexpression in the brain.

The neuropathological examination of the autopsy brain samples supported the postulated pathomechanism, showing that the lack of myelin and neuropathology occurred specifically in brain areas with *LMNB1* misexpression and consequent lamin B1 accumulation, as previously suggested.[5] In the atypical ADLD, only forebrain-derived regions (eg, cerebrum) were *LMNB1*-positive, and showed global white matter degeneration and astrocytes with foreshortened and beaded processes, whereas hindbrain-derived regions (eg, cerebellum and medulla oblongata) were preserved, in accordance with MRI findings (Fig 2). In these regions, *LMNB1* levels were negligible, suggesting that increased protein levels were more detrimental than decreased levels or no protein. These observations agree with the forebrain-midbrain specific pattern of misexpression proposed for all patients carrying inter-TAD deletions or duplications. Moreover, no dysautonomia in atypical ADLD could be explained by bulbar region preservation, which was responsible for autonomic functions, including breathing,[25] heart rate and blood pressure,[26] and the sleep–wake cycle.[27,28] Thus, intra-TAD duplications likely induce *LMNB1* overexpression in the overall brain, whereas atypical ADLD cases show a forebrain-midbrain overexpression owing to the adopted enhancers.

We identified a family carrying a large *LMNB1* inter-TAD duplication that extended centromerically and crossed 2 TAD boundaries (Figs 3D and S4B;

been stained with hematoxylin–eosin (HE), Lamin B1 (LMNB1), the astrocyte-specific marker glial fibrillary acidic protein (GFAP), and macrophage/monocytes marker (CD68). Tissues have been counterstained with Hematoxylin to visualize the nuclei. HE-stained tissue sections from the (A–C) frontal and (D–F) cerebellar white matter of a (A, D) healthy control, (B, E) classical ADLD patient, and (C, F) atypical ADLD patient show patchy lack of myelin and tissue rarefaction in the cerebrum of (B, C) both patients and (E) in the cerebellum of the classical ADLD case. (F) By contrast, the cerebellar white matter of the atypical ADLD patient is spared, with no lack of myelin nor tissue rarefaction. (G, J) Immunostain against *LMNB1* shows nuclear membranous immunoreactivity in a proportion of control white matter cells. (H, K) Classical ADLD shows similar findings. (I, L) In atypical ADLD, *LMNB1* expression in (I) frontal white matter is comparable to classical ADLD, whereas in the (L) cerebellum it is almost completely lost. Compared with (M, P) control white matter, (N, O) immunostaining against GFAP of the frontal lobe in both ADLD cases shows scattered dysmorphic astrocytes with short and blunt cell processes. By contrast, (Q) cerebellar white matter astrocytes are dysmorphic only in the classical ADLD patient, whereas (R) they retain a normal morphology in the atypical patient. Stain against CD68 shows sparse immunopositive macrophages in both (T, U) frontal and (W, X) cerebellar white matter from both ADLD cases, (S, V) with morphology similar to control cells. Scale bar = 50 μm.

Supplementary Material). The oldest *LMNB1* duplication carrier was a 68-year-old asymptomatic woman. The RNA-seq of whole-blood samples highlighted that all genes within the *LMNB1* locus were scarcely expressed compared with those in fibroblast samples, limiting the power of the analysis. However, *LMNB1* expression was strongly downregulated in the asymptomatic carrier compared with that in the control (Fig S6). The regulatory context of the resulting neo-TAD probably prevented *LMNB1* extra-copy expression in the brains of carriers, thus avoiding global white matter degeneration and disease manifestation. Interestingly, native and extra *LMNB1* copies maintained their physiological regulatory elements.[5]

A reevaluation of the literature and databases identified several large 5q duplications in the Decipher database, all were pediatric cases. However, we found 2 remarkable 5q23.2–23.3 duplications encompassing *LMNB1*.[29,30] Fonseca *et al*. reported a family with a 6.6-Mb insertional duplication encompassing *LMNB1* that translocated into chromosome 22.[29] Adult carriers (ranging from 46 to 77 years of age) showed neither demyelination at MRI nor clinical signs resembling ADLD. Luz *et al*. reported a second 3.2-Mb duplication encompassing *LMNB1*[30] in a pediatric patient with microcephaly. This rearrangement was inherited from the maternal grandmother. Both the mother and grandmother (aged 74 years) were healthy and showed normal MRIs. Unfortunately, these rearrangements were not characterized at the nucleotide level, limiting our ability to predict their effects on the 3D genome and TAD structure. In both families, the rearrangements probably moved the *LMNB1* extra copy in a peculiar regulatory context, preventing its expression in the brain.

We shed light on the 3D genome and TAD structure changes associated with SVs in the *LMNB1* locus, and demonstrated that a duplication encompassing *LMNB1* was not sufficient per se to diagnose ADLD. This finding has critical diagnostic consequences, because the extension of the duplication must be considered before confirming the causative role of a rearrangement involving *LMNB1*. Additionally, the present data suggested that astrocytic pathology covaried with the severity of neuropathology, indicating that astrocytes were a new and key pathological factor in ADLD. The functional consequences of *LMNB1* overexpression/misexpression may not only affect the expression of myelin genes, but can determine an astrocytic dysfunction negatively influencing oligodendrocyte homeostasis and myelin maintenance. Indeed, it has been shown that *LMNB1* overexpression induces a more severe morpho-functional sufferance of astrocytes compared with that of oligodendrocytes, which could affect their physiological functions owing to reduced astrocyte support.[9,31]

The present study showed the potential of Hi-C to detect and interpret SVs in a clinical setting using easily accessible cells obtained as part of routine diagnosis. In humans, the TAD structure at the *LMNB1* locus is well-conserved among tissues, supporting the use of fibroblasts to investigate how TAD structure is affected by different rearrangements. However, we could not exclude intra-TAD brain-specific contacts that were not detected in fibroblasts. Hi-C provided a resolution comparable to that of high-density arrays, allowing for the characterization of rearrangements and their functional outcomes. We foresee the possible use of Hi-C as a first-tier genetic test in genetic disorders to avoid the misinterpretation of asymptomatic *LMNB1* duplication carriers, which would occur when using gold-standard techniques, such as MLPA and aCGH.

In conclusion, the present results support breaking TADs as an emerging pathogenic mechanism that should be considered in diagnosing brain diseases and unveiling the genotype/phenotype correlation, which is ultimately indispensable for appropriate family counseling and patient care.

Author Contributions

E.G., M.S., P.C., and M.Bu. contributed to the conception and design of the study; E.G., P.D., M.Z., V.Y., U.S.M., J.H., A.Ba., I.C., C.T., R.L., F.D.K., G.R., L.M., F.P.E.V., M.B.D., G.V., M.Br., M.Bu., and E.B. contributed to the acquisition and analysis of data; E.G., P.D., M.Z., A.Ba., P.C., S.R., M.Bu., T.P., and A.Br. contributed to drafting the text or preparing the figures.

Potential Conflicts of Interest

Nothing to report.

Data Availability

Hi-C, RNA-seq, and WGS generated in this study are available under restricted access for patient privacy; access can be only obtained by request via data use agreements, which must be signed by our group and the applicant university/research institute. The processed Hi-C, RNA-seq, and WGS data are available upon request from E. Giorgio (elisa.giorgio@unipv.it) with the period for response to the access request of 1 calendar month. The processed data cannot be shared with third parties; if the data will be used for scientific presentations and/or publications, the applicant should contact E. Giorgio for further details. The raw sequencing data are protected and are not available due to data privacy laws. Data can only be shared for research purposes with permission of the patient's legal guardian(s). All other data supporting the findings described in this manuscript are available in the article, Supplementary Information.

References

1. Coffeen CM, McKenna CE, Koeppen AH, et al. Genetic localization of an autosomal dominant leukodystrophy mimicking chronic progressive multiple sclerosis to chromosome 5q31. Hum Mol Genet 2000;9:787–793. https://doi.org/10.1093/hmg/9.5.787.

2. Schuster J, Sundblom J, Thuresson AC, et al. Genomic duplications mediate overexpression of lamin B1 in adult-onset autosomal dominant leukodystrophy (ADLD) with autonomic symptoms. Neurogenetics 2011;12:65–72. https://doi.org/10.1007/s10048-010-0269-y.

3. Padiath QS, Saigoh K, Schiffmann R, et al. Lamin B1 duplications cause autosomal dominant leukodystrophy. Nat Genet 2006;38:1114–1123. https://doi.org/10.1038/ng1872.

4. Giorgio E, Rolyan H, Kropp L, et al. Analysis of LMNB1 duplications in autosomal dominant leukodystrophy provides insights into duplication mechanisms and allele-specific expression. Hum Mutat 2013;34:1160–1171. https://doi.org/10.1002/humu.22348.

5. Giorgio E, Robyr D, Spielmann M, et al. A large genomic deletion leads to enhancer adoption by the lamin B1 gene: a second path to autosomal dominant adult-onset demyelinating leukodystrophy (ADLD). Hum Mol Genet 2015;24:3143–3154. https://doi.org/10.1093/hmg/ddv065.

6. Nmezi B, Giorgio E, Raininko R, et al. Genomic deletions upstream of lamin B1 lead to atypical autosomal dominant leukodystrophy. Neurol: Genet 2019;5:e305. https://doi.org/10.1212/NXG.0000000000000305.

7. Heng MY, Lin ST, Verret L, et al. Lamin B1 mediates cell-autonomous neuropathology in a leukodystrophy mouse model. J Clin Invest 2013;123:2719–2729. https://doi.org/10.1172/JCI66737.

8. Bartoletti-Stella A, Gasparini L, Giacomini C, et al. Messenger RNA processing is altered in autosomal dominant leukodystrophy. Hum Mol Genet 2015;24:2746–2756. https://doi.org/10.1093/hmg/ddv034.

9. Ratti S, Rusciano I, Mongiorgi S, et al. Lamin B1 Accumulation's effects on autosomal dominant leukodystrophy (ADLD): induction of reactivity in the astrocytes. Cells 2021;10:2566. https://doi.org/10.3390/cells10102566.

10. Ibn-Salem J, Köhler S, Love MI, et al. Deletions of chromosomal regulatory boundaries are associated with congenital disease. Genome Biol 2014;15:423. https://doi.org/10.1186/s13059-014-0423-1.

11. Franke M, Ibrahim DM, Andrey G, et al. Formation of new chromatin domains determines pathogenicity of genomic duplications. Nature 2016;538:265–269. https://doi.org/10.1038/nature19800.

12. Flöttmann R, Kragesteen BK, Geuer S, et al. Noncoding copy-number variations are associated with congenital limb malformation. Genet Med 2018;20:599–607. https://doi.org/10.1038/gim.2017.154.

13. Kragesteen BK, Spielmann M, Paliou C, et al. Dynamic 3D chromatin architecture contributes to enhancer specificity and limb morphogenesis. Nat Genet 2018;50:1463–1473. https://doi.org/10.1038/s41588-018-0221-x.

14. de Bruijn SE, Fiorentino A, Ottaviani D, et al. Structural variants create new topological-associated domains and ectopic retinal enhancer-gene contact in dominant retinitis pigmentosa. Am J Hum Genet 2020;107:802–814. https://doi.org/10.1016/j.ajhg.2020.09.002.

15. Melo US, Piard J, Fischer-Zirnsak B, et al. Complete lung agenesis caused by complex genomic rearrangements with neo-TAD formation at the SHH locus. Hum Genet 2021;140:1459–1469. https://doi.org/10.1007/s00439-021-02344-6.

16. Meinel JA, Yumiceba V, Künstner A, et al. Disruption of the topologically associated domain at Xp21.2 is related to 46,XY gonadal dysgenesis. J Med Genet 2023;60:469–476. https://doi.org/10.1136/jmg-2022-108635.

17. Spielmann M, Lupiáñez DG, Mundlos S. Structural variation in the 3D genome. Nat Rev Genet 2018;19:453–467. https://doi.org/10.1038/s41576-018-0007-0.

18. Brunetti V, Ferilli MA, Nociti V, Silvestri G. Teaching NeuroImages: autosomal dominant leukodystrophy in a sporadic case. Neurology 2014;83:e121. https://doi.org/10.1212/WNL.0000000000000803.

19. Corazza I, Barletta G, Guaraldi P, et al. A new integrated instrumental approach to autonomic nervous system assessment. Comput Methods Programs Biomed 2014;117:267–276. https://doi.org/10.1016/j.cmpb.2014.08.002.

20. Zanigni S, Terlizzi R, Tonon C, et al. Brain magnetic resonance metabolic and microstructural changes in adult-onset autosomal dominant leukodystrophy. Brain Res Bull 2015;117:24–31. https://doi.org/10.1016/j.brainresbull.2015.07.002.

21. Lupiáñez DG, Kraft K, Heinrich V, et al. Disruptions of topological chromatin domains cause pathogenic rewiring of gene-enhancer interactions. Cell 2015;161:1012–1025. https://doi.org/10.1016/j.cell.2015.04.004.

22. Lupiáñez DG, Spielmann M, Mundlos S. Breaking TADs: how alterations of chromatin domains result in disease. Trends Genet 2016;32:225–237. https://doi.org/10.1016/j.tig.2016.01.003.

23. Melo US, Schöpflin R, Acuna-Hidalgo R, et al. Hi-C identifies complex genomic rearrangements and TAD-shuffling in developmental diseases. Am J Hum Genet 2020;106:872–884. https://doi.org/10.1016/j.ajhg.2020.04.016.

24. Dixon JR, Selvaraj S, Yue F, et al. Topological domains in mammalian genomes identified by analysis of chromatin interactions. Nature 2012;485:376–380. https://doi.org/10.1038/nature11082.

25. Zoccal DB, Furuya WI, Bassi M, et al. The nucleus of the solitary tract and the coordination of respiratory and sympathetic activities. Front Physiol 2014;5:238. https://doi.org/10.3389/fphys.2014.00238.

26. Kumagai H, Oshima N, Matsuura T, et al. Importance of rostral ventrolateral medulla neurons in determining efferent sympathetic nerve activity and blood pressure. Hypertens Res 2012;35:132–141. https://doi.org/10.1038/hr.2011.208.

27. Gottesmann C. The neurophysiology of sleep and waking: intracerebral connections, functioning and ascending influences of the medulla oblongata. Prog Neurobiol 1999;59:1–54. https://doi.org/10.1016/s0301-0082(98)00094-x.

28. Teng S, Zhen F, Wang L, et al. Control of non-REM sleep by ventrolateral medulla glutamatergic neurons projecting to the preoptic area. Nat Commun 2022;13:4748. https://doi.org/10.1038/s41467-022-32461-3.

29. Fonseca AC, Bonaldi A, Fonseca SA, et al. The segregation of different submicroscopic imbalances underlying the clinical variability associated with a familial karyotypically balanced translocation. Mol Cytogenet 2015;8:106. https://doi.org/10.1186/s13039-015-0205-9.

30. Luz D, Hogan K, Gordon L, Li M. eP181: expanding the phenotype of LMNB1 duplication: three generation family with microcephalic infant, asymptomatic individual, and eldest member without leukodystrophy. Genet Med 2022;24:S112. https://doi.org/10.1016/j.gim.2022.01.217.

31. Ratti S, Rusciano I, Mongiorgi S, et al. Cell signaling pathways in autosomal-dominant leukodystrophy (ADLD): the intriguing role of the astrocytes. Cell Mol Life Sci 2021;78:2781–2795. https://doi.org/10.1007/s00018-020-03661-1.